NMR Solution Structure of a Nonanucleotide Duplex with a dG Mismatch Opposite a 10*R* Adduct Derived from Trans Addition of a Deoxyadenosine N^6-Amino Group to (−)-(7*S*,8*R*,9*R*,10*S*)-7,8-Dihydroxy-9,10-epoxy-7,8,9,10-tetrahydrobenzo[*a*]pyrene†

Eric J. Schurter,‡ Herman J. C. Yeh,§ Jane M. Sayer,§ Mahesh K. Lakshman,§ Haruhiko Yagi,§ Donald M. Jerina,§ and David G. Gorenstein*,‡

Department of Chemistry, Purdue University, West Lafayette, Indiana 47907, and National Institutes of Diabetes and Digestive and Kidney Diseases, National Institutes of Health, Bethesda, Maryland 20892

Received February 4, 1994; Revised Manuscript Received September 14, 1994⊗

ABSTRACT: A nonanucleotide in which (−)-(7*S*,8*R*,9*R*,10*S*)-7,8-dihydroxy-9,10-epoxy-7,8,9,10-tetrahydrobenzo[*a*]pyrene (7-hydroxy group and epoxide oxygen are trans) is covalently bonded to the exocyclic N^6-amino group of deoxyadenosine through trans addition at C10 of the epoxide (10*R* adduct) has been synthesized. The modified oligonucleotide d(GGTCA*CGAG) was incorporated into the duplex d(GGTCA*CGAG)·d(CTCGGGACC), containing a dG mismatch opposite the modified base (dA*). Proton assignments for the solution structure of the duplex containing the 10*R* adduct were made using 2D TOCSY and NOESY NMR spectra. The complete hybrid relaxation matrix program, MORASS2.0, was used to generate NOESY distance constraints for iterative refinement using distance-restrained molecular dynamics calculations with AMBER4.0. The iteratively refined structure showed the hydrocarbon intercalated from the major groove immediately below the dC_4−dG_{15} base pair and oriented toward the 5′-end of the modified strand. The modified dA is in an anti configuration, with the dG of the GA mismatch turned out into the major groove. Chemical shifts of the hydrocarbon protons and unusual chemical shifts of sugar protons were accounted for by this orientation of the adduct. The information available currently provides the foundation for the rational explanation of observed benzo[*a*]pyrene (BaP) structures and predictions for other BaP dG and dA adducts.

Alternant polycyclic aromatic hydrocarbons are widespread environmental contaminants whose metabolism in mammals often results in the formation of carcinogenic, benzo ring bay-region diol epoxides (Jerina et al., 1988). Since it is believed that the initiating event in cell transformation induced by these diol epoxides involves the formation of a covalent bond between a nucleophilic group in DNA and the benzylic carbon atom of the epoxide, the structures of the adducts thus formed are of considerable interest. Enzymatic degradation of DNA covalently modified by diol epoxides has led to the identification [reviewed in Jerina et al. (1991)] of the exocyclic amino groups of purine nucleosides deoxyguanosine (dG) and deoxyadenosine (dA) as the major sites of attachment of the diol epoxide moieties to DNA, although deoxycytidine adducts and endocyclic N-7 dG adducts are also observed. Since the formation of diol epoxides in mammals involves the epoxidation of *trans*-dihydro diol intermediates, two stereoisomeric diol epoxides are possible, namely, the diol epoxide 1 (syn) diastereomer in which the benzylic hydroxyl group and the epoxide oxygen are cis and the diol epoxide 2 (anti) diastereomer in which these two groups are trans. For each of these diastereomers, two enantiomers are possible. Ring opening of diol epoxides at the benzylic carbon atom occurs by the approach of a nucleophile from either the same face of the molecule as the oxirane oxygen or from the opposite face (to give cis or trans opened adducts, respectively). Thus, eight dA and eight dG adducts are possible. The two diol epoxide 2 (DE2) enantiomers derived from benzo[*a*]pyrene (BaP) and the adducts formed upon trans ring opening of these epoxides by the exocyclic 6-amino group of dA are shown in Figure 1.

Despite the accumulation of substantial data (Jerina et al., 1991) on the reactivity of diol epoxides with DNA and on the structures of the nucleoside adducts formed, analysis of these data has provided no obvious correlation with tumorigenicity. Thus, neither overall chemical reactivity, efficiency of covalent binding to DNA as opposed to hydrolysis, nor the relative proportions of dG vs dA adducts or of cis vs trans epoxide ring opening are clearly correlated with the tumorigenicity of specific diol epoxides. It is apparent that detailed structural analysis of these adducts at the oligonucleotide level is required to elucidate their interactions with the enzymes involved in DNA replication and repair.

To this end, solution structures have been investigated by NMR for three adducts formed from oligonucleotides of defined sequence upon reaction with the enantiomers of BaP-

† We thank NIH-NCI Training in Drug and Carcinogen-DNA Interactions (Grant CA09634), the NIH (Grant AI27744), and the Purdue University Biochemistry Magnetic Resonance Laboratory, which is supported by the NSF Biological Facilities Center on Biomolecular NMR, Structure and Design at Purdue (Grants BBS8614177 and DIR-9000360 from the Division of Biological Instrumentation).

* Address correspondence to this author at the Department of Human Biological Chemistry and Genetics, University of Texas Medical Branch, Galveston, TX 77555.

‡ Purdue University.

§ National Institutes of Health.

⊗ Abstract published in *Advance ACS Abstracts,* November 1, 1994.

0006-2960/95/0434-1364$09.00/0

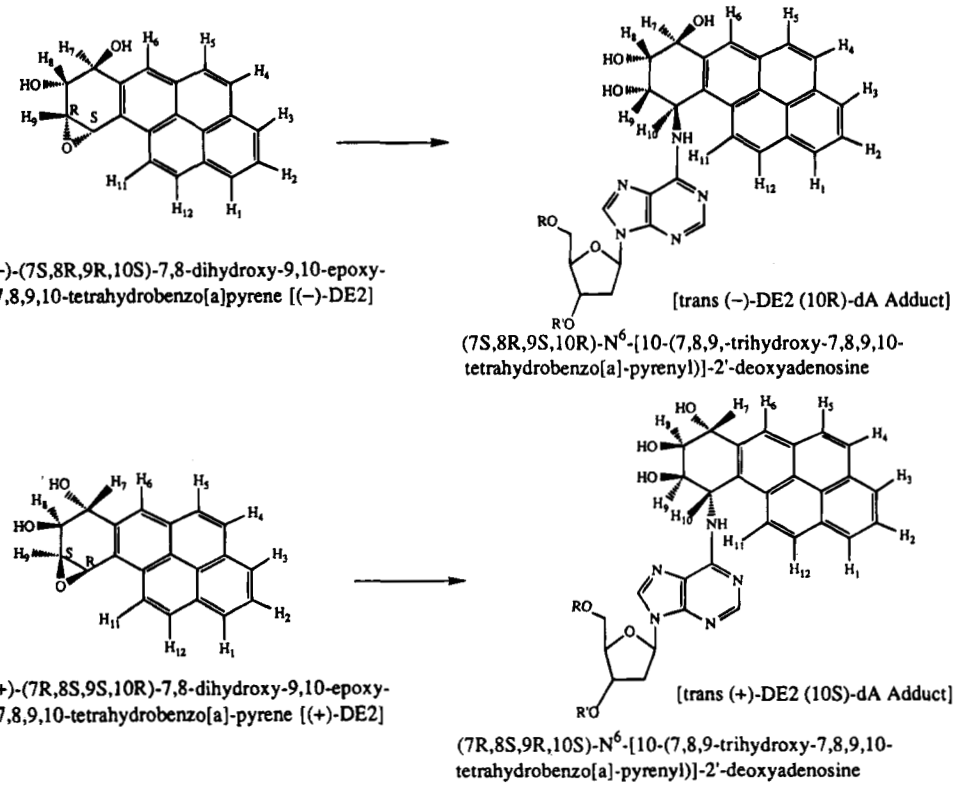

FIGURE 1: Trans addition of the exocyclic N^6-amino group of dA to the enantiomers of (±)-7β,8α-dihydroxy-9α,10α-epoxy-7,8,9,10-tetrahydrobenzo[*a*]pyrene (BaP-DE2). Since the adducts arise by trans addition, the configuration at C10 is inverted when comparing the diol epoxide to the adduct. A corresponding change in configurational designation also occurs at C9, in this case due to application of the priority rules rather than a change in configuration.

DE2 (Cosman et al., 1992, 1993a; de los Santos et al., 1992), as well as with one enantiomer of the same diastereomeric benzo[*c*]phenanthrene-(BcPh)-3,4-diol 1,2-epoxide 2 (Cosman et al., 1993b). Whereas the BcPh-modified oligonucleotide involves modification of a dA residue at its exocyclic 6-amino group, the three structures determined for BaP-modified oligonucleotides all involved dG adducts. Although dG adducts quantitatively are the most significant ones formed from DNA in vitro at high, nonphysiological concentrations of the highly carcinogenic (+)-BaP-DE2 (Figure 1), there is no reason to conclude that these are the adducts primarily responsible for cell transformation and carcinogenesis. At high doses, this BaP-diol epoxide induces mutations primarily at dG. At lower, more environmentally and physiologically realistic doses, mutations at dA become much more significant (Wei et al., 1991, 1993, 1994). Thus, the structures of oligonucleotides containing BaP-diol epoxide adducts at dA, which are less accessible than the dG adducts by direct reaction of the diol epoxides with oligonucleotides, are of considerable interest.

The present report describes the structure of the duplex $d(G_1G_2T_3C_4A^*{}_5C_6G_7A_8G_9)\cdot d(C_{10}T_{11}C_{12}G_{13}G_{14}G_{15}A_{16}C_{17}C_{18})$ in which the dA* residue represents the 10*R* dA adduct formed from (−)-DE2 (Figure 1). This represents the first NMR structure of an oligonucleotide containing a BaP adduct at dA, as well as the first such structure of a BaP adduct with a base other than the normal complement opposite the adduct. As will be detailed here, the duplexes with dG opposite the modified dA residues were selected mainly due to T_m considerations. Although the biological significance of base mispairing in BaP-modified DNA is not clearly established, it might well provide a mechanism for the A→C transversion mutations that are observed in the *HPRT* gene of Chinese hamster V-79 cells at low doses of BaP-diol epoxide 2 (Wei et al., 1993, 1994).

EXPERIMENTAL PROCEDURES

Sample Preparation. The major products formed upon reaction of DNA with the diol epoxides derived from BaP result from the modification of dG residues. Thus, direct reaction (Cosman et al., 1990) of oligonucleotides with the diol epoxides is not a practical route to significant quantities of oligonucleotides specifically modified at dA residues. Consequently, the previously described synthetic approach (Lakshman et al., 1992) for the preparation of diol epoxide-adducted dA phosphoramidites and their incorporation into oligonucleotides was used. Two nonanucleotides, d(GGTCA*CGAG), were synthesized using modifications of this method: one in which the central adduct has 10*R* absolute configuration at the benzylic carbon atom of the hydrocarbon and corresponds to trans opening of the (−)-(7*S*,8*R*,9*R*,10*S*)-DE2 isomer by N^6 of dA, and the other which has 10*S* absolute configuration at this center and corresponds to the same trans opening of the enantiomeric (+)-(7*R*,8*S*,9*S*,10*R*)-DE2 (Figure 1). Full details of the syntheses will be published elsewhere.

Stoichiometry for duplex formation from the modified oligonucleotides was determined most conveniently by spectrophotometric titration of a sample of the modified oligonucleotide with its partially complementary strand, d(CTCGGGACC). The addition of aliquots of a solution of the complementary strand to the modified oligonucleotide at 5 °C in a buffer (100 mM total ionic strength) containing 12 mM Na_2HPO_4, 8 mM NaH_2PO_4, and 56 mM NaCl at pH 7 gives rise to a pronounced red shift and hypochromicity

of the long wavelength bands of the pyrene chromophore upon duplex formation. This spectral change, which occurs instantaneously, is far from the wavelength maximum for DNA; thus, the titration end point is easily obtained from the point at which addition of the complementary oligonucleotide produces no further spectral change. From the titration of a small portion of the modified oligonucleotide, the proper ratio for mixing of the two oligonucleotide solutions in the NMR sample was determined; this corresponded to approximately 0.8 A_{260} unit of complementary strand to 1 A_{260} unit of adducted strand. The sample used for the NMR studies contained approximately 172 A_{260} units of duplex and was dissolved in 600 μL of D_2O (99.995%) buffer (100 mM total ionic strength) containing 12 mM Na_2HPO_4, 8 mM NaH_2PO_4, 56 mM NaCl, and 2 mM sodium azide adjusted to pH 7 with NaOD. The purity of the sample was verified by HPLC, and the NMR spectra showed no indication of sample degradation over time.

NMR Experiments. A Varian VXR500 (500 MHz) spectrometer at a regulated temperature of 15 °C was used to record the 2D TOCSY and NOESY spectra. The TOCSY spectra (Bax & Davis, 1985; Braunschweiler & Ernst, 1983) were recorded at 50 and 100 ms mixing times. The NOESY spectra were recorded at 100, 150, and 300 ms mixing times. All spectra were acquired with 4096 complex points in the t_2 dimension and 1024 complex t_1 increments and then apodized with a shifted sine bell before Fourier transformation. NOESY volumes were taken from the 150 ms mixing time spectra for structural refinement. The base proton to H1′NOESY cross-peak intensities were used to distinguish qualitatively between the syn (strong NOE) and anti (weak NOE) glycosidic torsional angles (Wüthrich, 1986).

NOESY Distance-Restrained Molecular Mechanics/Dynamics Calculations of DNA−Benzo[a]pyrene Adduct. The Chem3D 3.0 (Cambridge Scientific Computing, Inc.) program was used to generate bond distances, bond angles, and dihedral angles for the (10*R*)-dA adduct. The force field parameters were adopted from equivalent AMBER4.0 atom types (Weiner & Kollman, 1981), and the partial molecular charges were from ab initio calculations (Hingerty & Broyde, 1985). The AMBER4.0 molecular dynamics program was then used on a Silicon Graphics Indigo XS24 R4000 workstation to generate the duplex B-DNA containing the adduct. The MIDAS Plus molecular modeling program (Langridge & Ferrin, 1984) was used to manipulate manually the starting model structures and to display the refined structures. The hybrid complete relaxation matrix program, MORASS2.0 (Gorenstein et al., 1993), was used to generate a total of 189 NOESY flat-well distance constraints for iterative refinement using distance-restrained molecular dynamics calculations with a locally modified version of AMBER4.0.

Th MORASS program (multiple Overhauser relaxation analysis and simulation) was used to calculate volume and rate matrices, as well as implement the hybrid matrix methodology. Typically, the well-resolved and measurable cross peaks in the NOESY spectrum replace the corresponding cross peaks in the calculated volume matrix, while overlapping or weak cross peaks and diagonals are retained from the calculated spectrum. This hybrid volume matrix, V_{hyb}, is then used to evaluate the rate matrix whose off-diagonal elements include the effects of spin diffusion.

Table 1: Melting Temperatures of Normal d(GGTCACGAG) and Modified Oligonucleotides with the Fully or Partially Complementary Strands d(CTCGXGACC) as a Function of the Base, X, Opposite the Central Deoxyadenosine Residue[a]

	T_m		
X	unmodified duplex[b]	*trans*-(−)-DE2−(10*R*)-dA adduct[c]	*trans*-(+)-DE2−(10*S*)-dA adduct[c]
T	43	28	16
G	36	27	28
A	25	21	20

Distances derived from the hybrid relaxation rate matrix (we assume a single isotropic correlation time of 2.7 ns) are then utilized as constraints in a 6 ps restrained molecular dynamics simulation. Energy minimization of the averaged last 3 ps structures, derived from molecular dynamics, completes one cycle of refinement. This process is repeated until satisfactory agreement between the calculated and observed cross-peak volumes is obtained. As shown by our laboratory (Nikonowicz et al., 1989, 1990; Gorenstein et al., 1990; Kaluarachchi et al., 1991) and others (Boelens et al., 1988, 1989; James et al., 1991), 3−5 iterations appear to be adequate to achieve convergence to a refined structure.

Convergence is monitored by using the equation

$$\%\mathrm{RMS}_{vol} = \{[(1/N)\sum[(v_{ij}^{a} - v_{ij}^{b})/v_{ij}^{a}]^2]\}^{1/2} \times 100 \quad (1)$$

where $\%\mathrm{RMS}_{vol} = \%T$ when v^a is the calculated volume and v^b is the experimental volume, and $\%\mathrm{RMS}_{vol} = \%E$ when v^a is the experimental volume and v^b is the calculated volume. Convergence is achieved when the RMS deviation in percentage volumes ($\%\mathrm{RMS}_{vol}$) is within the reliability of the experimental volume measurement. Since most structurally important distances are those from longer range NOEs, and since these small off-diagonal volumes (<2% of the diagonal volumes) are the most sensitive to experimental noise, we feel that an acceptable %RMS error is 50−60%. The *R*-factor is also monitored and is slightly smaller (50%) because the short fixed distances make a major contribution to this value. A 60% error in the average volume represents only a 10% error in the average distances due to the r^{-6} distance dependence of the NOE volume.

All energy minimization and restrained molecular dynamics calculations were done in vacuo with a distance-dependent dielectric to simulate bulk solvation by water. The molecular dynamics (MD) calculations were run in 6 ps blocks. The temperature was started at 100 K and raised to 400 K over 1 ps. Then the temperature was reduced to 300 K over 2 ps and maintained for the remaining 3 ps of the MD run. The coordinates for the last 3 ps of the MD run were averaged, followed by 300 cycles of minimization.

RESULTS

Melting Temperatures of Benzo[a]pyrene−DNA Adducts. Upon annealing the two nonamers containing the dA adducts with 10*R* and 10*S* absolute configuration (Figure 1) with their complementary strands (see Table 1), it became clear that the duplex formed from the strand containing a (10*S*)-dA adduct [derived from the highly carcinogenic (+)-(BaP-(7*R*,8*S*,9*S*,10*R*)-DE2 with its normal complementary strand, d(CTCGTGACC)] had a surprisingly low T_m and that the presence of a dG residue opposite the modified dA increased

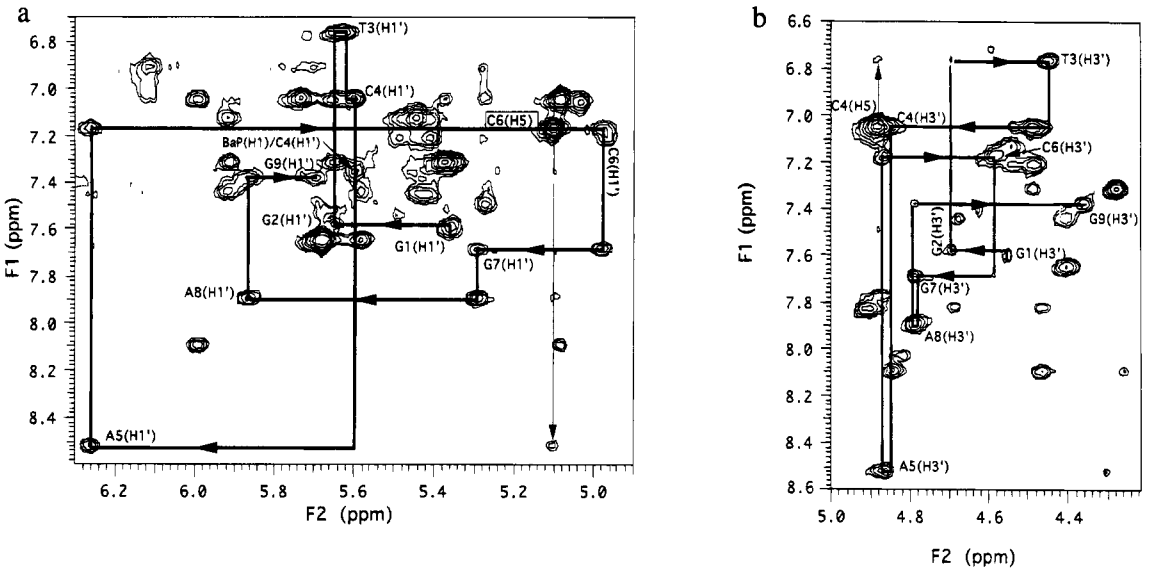

FIGURE 2: Expanded NOESY spectra (150 ms mixing time) showing the connectivities between the base protons (8.6 to 6.6 ppm) and sugar (a) H1′ (6.3 to 4.9 ppm) or (b) H3′ (4.9 to 4.4 ppm) protons. The connectivities depicted are for the modified strand. The dC H5 to base connectivities are indicated with vertical arrows. The dC_4 (H1′, 5.63 ppm) to dA_5 (H8, 8.54 ppm) cross peak is very weak but clearly observable in the 300 ms NOESY spectra. Cross peaks between the H1 proton of the BaP moiety (BaP(H1), 7.39 ppm) and dC_4 (H1′, 5.63 ppm), which help establish the intercalated orientation of the hydrocarbon, are also shown.

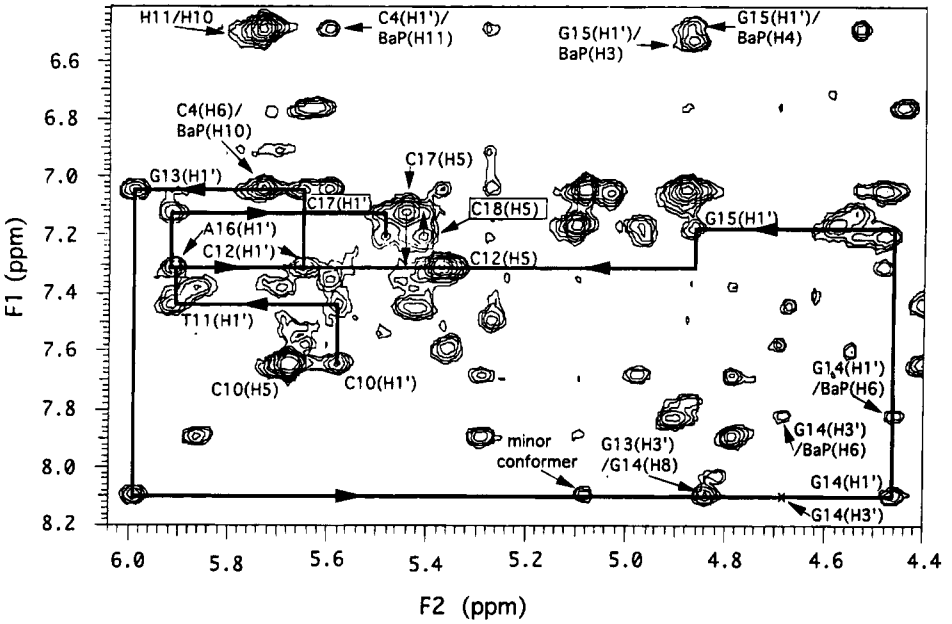

FIGURE 3: Expanded NOESY spectrum (150 ms mixing time) showing the connectivities between the base protons (8.6 to 6.6 ppm) and sugar H1′ (6.3 to 4.5 ppm) protons. Connectivities depicted are for the complementary strand, with cross peaks between the hydrocarbon protons and sugar protons indicated. The dC_5 to base connectivities are indicated with arrows. The dG_{15} (H1′, 4.90 ppm) to dA_{16} (H8, 7.34 ppm) cross peak is not observable. Cross peaks between BaP (H11, 6.52 ppm) and dC_4 H1′, 5.63 ppm), BaP (H4, 6.50 ppm) and dG_{15} (H1′, 4.90 ppm), BaP (H3, 6.56 ppm) and dG_{15} (H1′, 4.90 ppm), and BaP (H6, 7.85 ppm) and dG_{14} (H3′, 4.68 ppm; H1′, 4.49 ppm) show that the hydrocarbon is intercalated.

the T_m of this duplex by 12 °C (Table 1). In contrast, duplexes with either dT or dG opposite the (10*R*)-dA adduct [derived from the enantiomeric BaP-(−)-(7*S*,8*R*,9*R*,10*S*)-DE2] had virtually identical T_m values, which were also the same as the T_m for the (10*S*)-dA adduct with a dG opposite the modified base.

Nonexchangeable DNA Proton Spectra. Through-bond connectivities in the TOCSY spectra were used to identify sugar spin systems, and through-space NOE cross peaks from the NOESY spectra were used to establish the base connectivities along each DNA strand. Figure 2a,b shows the connectivities for the modified strand in the H1′,H3′ to base proton region. The connectivities were completely traced through the H1′ to base region with a very weak NOE between dC_4 (H1′) and dA_5 (H8), reflecting local distortions due to the dA_5-bound hydrocarbon. By D_2O exchange into the H8 protons of the purines, we were able to confirm that the unusual downfield-shifted resonance at 8.54 ppm is H8 and not H2 of the modified base dA_5. This confirms that the modified base is in an anti conformation. Figure 3 shows the connectivities for the complementary strand. The connectivities show a break between dG_{14} and dG_{15} and between dG_{15} and dA_{16} due to large distortions induced by the hydrocarbon ring system. The H1′, H3′, H6, and H8

Table 2: Chemical Shift Assignments for the (10*R*)-dA Adduct Sugar Protons (in ppm) Referenced to H_2O (4.65 ppm at 15 °C)[a]

modified strand	H1′	H2′	H2″	H3′	H4′	H6 or H8	H5	H2	H5′,H5″	Me
5′-Gua 1	5.38	2.30	2.42	4.57	4.40	7.61			3.42, 3.93	
5′-Gua 2	5.66	2.37	2.37	4.72	4.12	7.60			3.85, 3.92	
5′-Thy 3	5.67	1.30	1.55	4.48	4.38	6.79			3.80, 3.90	1.00
5′-Cyt 4	5.63	2.16	2.23	4.91	4.67	7.07	4.88		3.80, 4.06	
5′-Ade 5[b]	6.29	2.79	2.86	4.89	4.32	8.54			3.98, 3.82	
5′-Cyt 6	5.01	1.83	2.01	4.60	3.91	7.18	5.12		3.90, 3.96	
5′-Gua 7	5.31	2.54	2.58	4.78	4.10	7.71			3.74, 3.88	
5′-Ade 8	5.89	2.46	2.68	4.82	4.18	7.92			3.90, 4.02	
3′-Gua 9	5.71	2.01	2.15	4.39	3.90	7.40			3.88, 4.02	
complementary strand	H1′	H2′	H2″	H3′	H4′	H6 or H8	H5	H2	H5′,H5″	Me
5′-Cyt 10	5.61	2.03	2.35	4.48	3.86	7.67	5.69		3.92	
5′-Thy 11	5.94	2.58	2.38	4.70		7.46			3.84, 4.04	1.46
5′-Cyt 12	5.68	1.68	2.16	4.52	3.90	7.33	5.39		3.78, 3.90	
5′-Gua 13	6.02	2.64	2.64	4.87	4.28	7.07			3.92, 4.08	
5′-Gua 14	4.49	2.41	2.55	4.68	4.28	8.11			3.90, 4.14	
5′-Gua 15	4.90	2.49	2.34	4.63		7.19			3.81	
5′-Ade 16	5.91	1.97	2.04	4.30	3.78	7.34			3.76, 3.91	
5′-Cyt 17	5.51	1.89	1.48	4.56	3.80	7.16	5.47		3.70, 3.80	
3′-Cyt 18	4.98	1.28	1.07	4.51	3.68	7.23	5.43		3.69, 3.92	

[a] Missing chemical shifts could not be unambiguously assigned. The H5′,H5″ protons could not be distinguished and are listed in random order. [b] Ade 5: the adducted base derived from (−)-BaP−(7*S*,8*R*,9*R*,10*S*)-DE2 as shown in Figure 1.

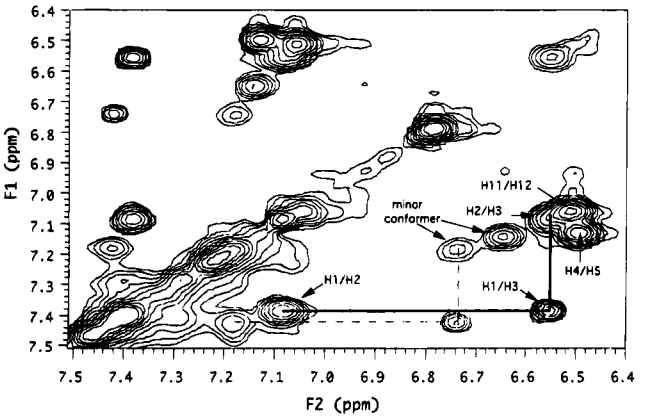

FIGURE 4: Expanded TOCSY spectrum (50 ms mixing time) showing the cross peaks for the aromatic protons of the (10*R*)-dA adduct (H1, 7.39 ppm; H2, 7.09 ppm; H3, 6.56 ppm; H4, 6.50 ppm; H5, 7.13 ppm; H11, 6.62 ppm; H12, 7.07 ppm). The solid line indicates the three-spin system [BaP(H1, H2, and H3)]. The dashed line indicates the corresponding three-spin system observed for the minor conformer, with integrated volumes 20% of the major conformer.

Table 3: Chemical Shift Assignments for the Hydrocarbon Protons of the (10*R*)-dA Adduct in DNA (in ppm) Referenced to H_2O (4.65 ppm at 15 °C)[a]

tetrahydrobenzopyrene protons	chemical shift assignments
H1	7.39
H2	7.09
H3	6.56
H4	6.50
H5	7.13
H6	7.85
H7	5.29
H8	4.40
H9	4.56
H10	5.75
H11	6.52
H12	7.07

[a] 7,8,9,10-Tetrahydrobenzo[*a*]pyrene protons H1, H2, H3, H4, H5, H6, H11, and H12 are aromatic, with the remainder aliphatic (H7, H8, H9, and H10).

assignments were confirmed using several regions of the spectra, with the complete assignments for the base, H1′, H2′, H2″, and H3′ protons shown in Table 2.

Nonexchangeable Protons of the Hydrocarbon. Through-bond connectivities in the TOCSY spectra were used to identify the coupled spin systems of the hydrocarbon, and through-space NOE cross peaks from the NOESY spectra were used to connect the spin systems. Figure 4 shows the aromatic protons of the hydrocarbon. The structure, labeling convention, and absolute configuration for the (10*R*)-dA adduct are shown in Figure 1, with the complete assignment of all protons of the hydrocarbon given in Table 3. NOE cross peaks due to a 20% fraction of a minor conformer were distinguishable by ratioing the volumes of peaks in corresponding spin systems (4:1 major to minor conformer; see supplementary material Figure 1S). The minor conformer is in slow exchange, and only a few of the most intense minor conformer cross peaks were identifiable in uncongested regions of the spectra. Slow exchange is not unexpected because of steric limitations on the mobility of the hydrocarbon due to its size. No structural assignment for the minor conformer was possible.

NOESY Cross Peaks between the Hydrocarbon and DNA Protons. The orientation of the hydrocarbon in the (10*R*)-dA adduct was proved by NOE cross peaks between the protons on the hydrocarbon and adjacent DNA sugar protons. Each side of the tetrahydro-BaP ring system had NOEs to opposite strands of the DNA duplex, consistent with an intercalated orientation. For example, hydrocarbon protons H1 and H11 are on the same edge of the pyrene ring system and have cross peaks to dC_4 sugar protons on the modified strand (Figure 5 and Figures 2S and 3S of the supplementary material). In contrast, hydrocarbon protons H3 and H4 are on the other edge of the ring system and have NOEs to dG_{15} sugar protons on the unmodified strand (Figure 5).

Chemical Shifts. A large upfield chemical shift for dG_{14}-(H1′) to 4.49 ppm was observed. This can be accounted for by base stacking over the tetrahydro-BaP ring system (Figure 6). More dramatic chemical shifts of H1′ protons due to this hydrocarbon ring system have been reported by de los Santos et al. (1992). They observed a H1′ proton

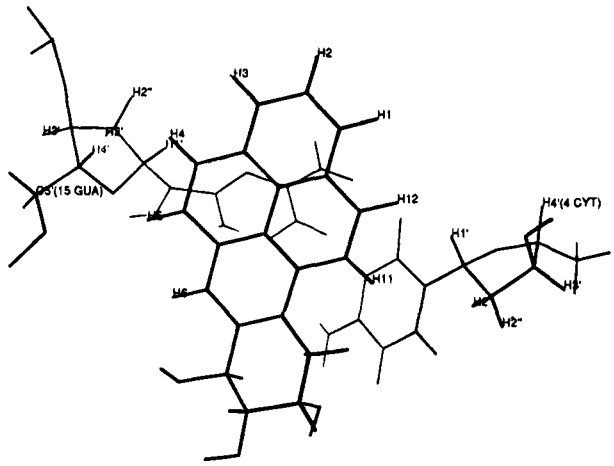

FIGURE 5: Refined structure of the (10*R*)-dA adduct in DNA (view along helical axis, 5′-direction of modified strand). The refined structure shows the proximity of dC_4 (modified strand) sugar protons to BaP H1 and H11 protons for which NOE cross peaks are observable. NOEs to BaP H12 and dC_4 sugar protons are overlapped. The location of hydrocarbon protons (H4, H3) relative to dG_{15} (complementary strand) sugar protons is supported by observable NOEs. dG_{15} (H1′, 4.90 ppm) is partially stacked under the pyrene rings accounting for its upfield chemical shift.

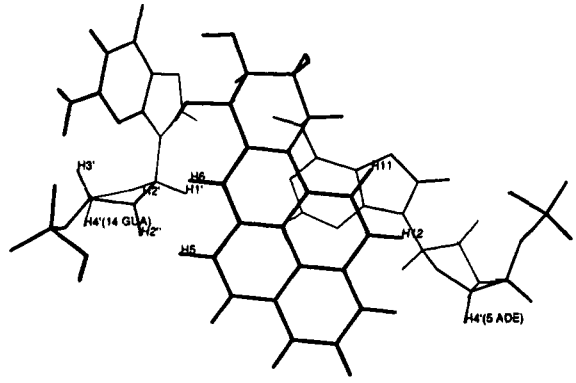

FIGURE 6: Refined structure of the (10*R*)-dA adduct in DNA (view along helical axis, 3′-direction of modified strand). The refined structure shows only the H1′ (4.49 ppm) of dG_{14} sugar protons stacked under the pyrene ring system, resulting in a large upfield chemical shift for H1′. The large upfield chemical shift for the aromatic proton H11 (6.52 ppm) can be accounted for by its stacking over the base of dA_5, the residue that is covalently modified by the hydrocarbon.

shifted upfield by the hydrocarbon ring in a *trans*-(−)-DE2 (10*R*)-dG adduct in a DNA duplex. The peaks at 5.1 and 8.1 ppm cannot involve this proton in the major conformational isomer present since they belong to the minor conformer. This was easily varified because the proton at 5.1 ppm has no cross peaks to any of the other dG_{14} sugar protons (H2′, H2″, H3′, H4′, H5′, or H5″) and no TOCSY cross peaks to any protons in the H2′,H2″ region. The assigned dG_{14} (H1′, 4.49 ppm) has TOCSY and NOESY cross peaks to dG_{14} protons [H2′(2.41 ppm), H2″(2.55 ppm), and H3′ (4.68 ppm)]. dG_{15}(H1′) showed a more moderate upfield shift to 4.90 ppm due to the proximity of the hydrocarbon (Figure 5). The nonexchangeable protons on the hydrocarbon showed a chemical shift pattern similar to that observed for the intercalated structure of the *cis*-(+)-DE2 (10*R*)-dG adduct (Cosman et al., 1993a). For the aromatic protons, these shifts are all upfield compared to those for the pyrene moiety located in the minor groove of oligonucleotides containing *trans*-DE2 (10*R*)- and (10*S*)-dG

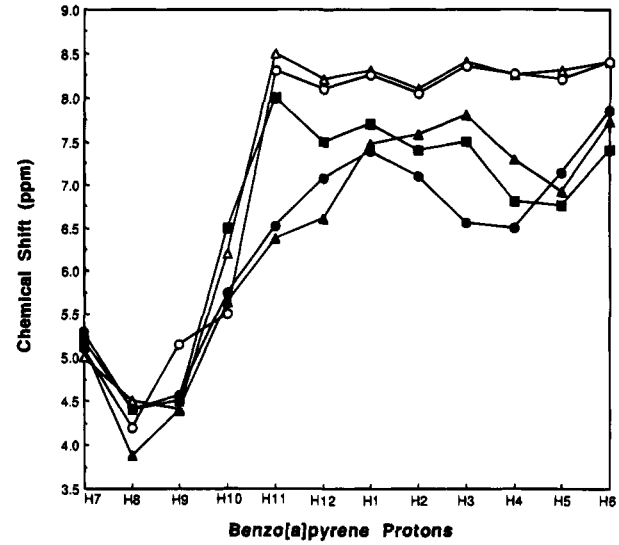

FIGURE 7: Nonexchangeable protons of the tetrahydro-BaP moiety plotted against chemical shift. Plot compares the intercalated *trans*-(−)-De2−(10*R*)-dA adduct (●) of this study, the intercalated *trans*-(+)-DE2−(10*S*)-dA adduct (▲) (unpublished results), and the intercalated *cis*-(+)-DE2−(10*R*)-dG adduct (■) solved by Patel. The *trans*-(+)-DE2−(10*S*)-dG (△) and *trans*-(−)-DE2−(10*R*)-dG (○) adducts have the hydrocarbon oriented in the minor groove. Note the unusual chemical shift of H11 (6.52 ppm).

adducts (Figure 7) (Cosman et al., 1992; de los Santos et al., 1992). The unusually large upfield shift of H11 of the hydrocarbon can be accounted for by its position directly over the dA_5 base and under the dC_4 base (5′-end of the modified strand orients the top of the duplex) (Figures 5 and 6).

Exchangeable Proton Spectra. Water/NOESY spectra were run at 100 and 200 ms mixing times at 15 and 5 °C to evaluate the exchangeable protons. However, the spectra of 15 °C showed strong magnetization transfer to water, with a resulting reduction in cross-peak intensity. When the temperature was reduced there was a modest increase in cross-peak intensity; however, many of the proton chemical shifts changed. Therefore, it was not possible to unambiguously assign the exchangeable protons due to the combined effect of very weak exchangeable NOESY cross peaks and temperature-induced chemical shifts.

Structural Refinement of the Adduct. Eight different starting model structures were considered with B-DNA backbones and various orientations of the hydrocarbon ring system. Four starting structures with the hydrocarbon in the major or minor groove, oriented toward the 5′- or 3′-end of the modified strand, were eliminated from consideration. None of these structures could satisfy all of the observed NOEs between the protons of the hydrocarbon and the sugars in the DNA duplex. The two starting structures with the hydrocarbon intercalated from the minor groove and the base of dG_{14} turned out resulted in severe kinking of the DNA backbone as the hydrocarbon moiety pulled out into the major groove and began to reinsert during the course of refinement.

The remaining two starting models both had the hydrocarbon intercalated from the major groove. They differed in whether the base of dG_{14} (dG of the GA mismatch) was stacked in with the hydrocarbon or turned out into the major groove. Structural refinement of both starting models yielded structures with the base of dG_{14} maintaining its approximate

Table 4: MORASS/Molecular Dynamics Iterative Refinement Cycles for the Final Structure (The Refinement Was Started with Model-Built Coordinates)

iteration	flat well[a]	% error[b]	H bond[c]	Ade 5 H2′,H2″ to Ade H8[d]	Gua 14 H1′ to BP H6[e]	RMS[f]	%E[g]	%T[h]	R-factor[i]	unconstrained energy[j]	constraint energy[k]
model						1.62	221	553	0.52		
1	3	18	15	6		1.24	236	132	0.50	−707	13.5
2	4	16	17	8		0.87	284	113	0.52	−717	13.8
3	5	14	16	10	10	0.45	275	91	0.52	−712	22.7
4	6	12	16	12	12	0.24	268	92	0.50	−704	43.1
5	6	10	16	12	12	0.19	102	73	0.45	−706	30.6
6	8	10	16	12	12	0.20	77	69	0.44	−697	34.0
7	15	10	16	15	15	0.20	64	64	0.42	−690	31.0

[a] Harmonic potential force constant (kcal mol^{-1} Å^{-2}) applied to the flat-well contraints. [b] Half the percent variation in the constraint distance allowed without energy penalty. [c] Hydrogen-bonding constraint energy between base pairs. [d] Harmonic potential force constant (kcal mol^{-1} Å^{-2}) applied to the flat-well constraint energy for Ade 5 (H2′) to Ade 5 (H8) and for Ade 5 (H2″) to Ade 5 H8). [e] Harmonic potential force constant (kcal mol^{-1} Å^{-2}) applied to the flat-well constraint energy for Gua 14 (H1′) to benzopyrene (H6). [f] Root mean square error in volumes calculated by MORASS. [g] Average error in volumes [(exp − theoretical)/exp] calculated by MORASS. [h] Average error in volumes [(theoretical − exp)/theoretical] calculated by MORASS. [i] The *R*-factor is calculated with the following equation, where v_{ij}^a is the experimental volume measurement and v_{ij}^b is the calculated volume: *R*-factor = $\{\Sigma[v_{ij}^a - v_{ij}^b]\}/\Sigma[v_{ij}^a]$. [j] Total energy of the structure not including the NOESY distance constraint term. [k] Total energy of NOESY distance constraints.

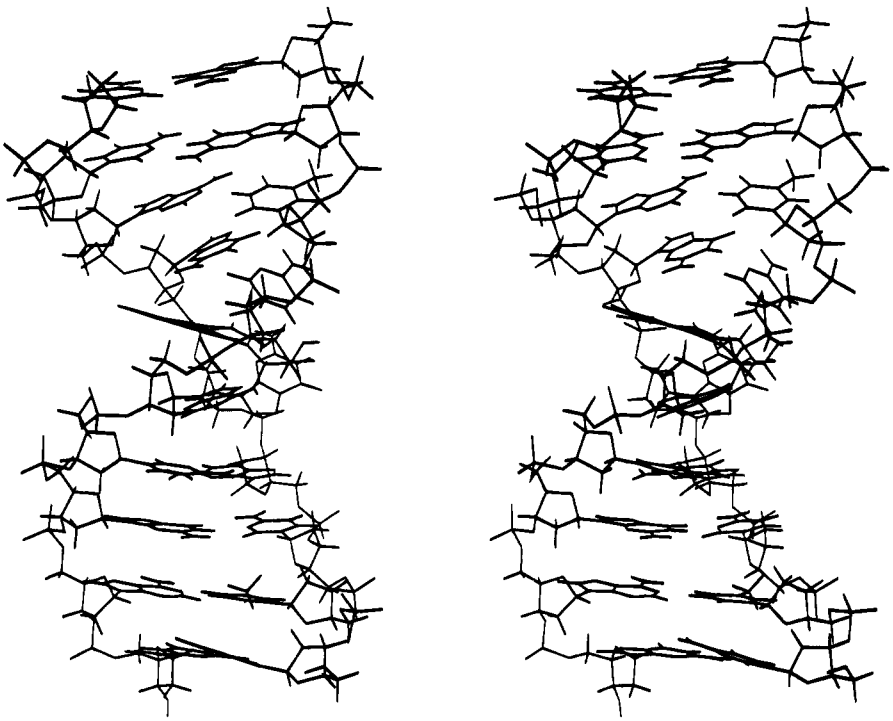

FIGURE 8: Stereoview of the (10*R*)-dA adduct in DNA with the 5′-end of the modified strand at the top.

starting position. In both cases, the hydrocarbon remained intercalated under the dG_{15}−dC_4 base pair. The structure with dG_{14} stacked in the duplex could be eliminated because the MORASS NOESY spectral simulation produced strong NOEs between its H8 and the protons of the hydrocarbon that were not observed in the experimental NOESY spectra. Refinement of the model with dG_{14} turned out into the major groove did not result in any NOEs that were at variance with the experimental NOESY spectra.

The progress of the iterative MORASS/MD structural refinement starting with the hydrocarbon intercalated from the major groove and the base of dG_{14} turned out into the major groove is shown in Table 4. The final structure resulted in an approximately 64% RMS percentage peak volume deviation between the theoretical and experimental volumes. The %RMS deviation reflects the increased uncertainty in the volumes due to overlap with the 20% minor conformer present. Isolated minor conformer cross peaks were distinguishable from major conformer cross peaks because minor conformer protons had very few or no observable NOE connectivities. Further, slow exchange resulted in there being no NOE cross peaks between the major and minor conformers. All volumes merged after the fifth iteration, and the total constraint energy penalty was 31 kcal/mol·Å^2. There were 189 NOE distance constraints incorporated into the refinement, with 16 of those between nonexchangeable hydrocarbon protons and DNA duplex sugar protons.

A side view of the final refined structure is shown in Figure 8. The DNA helical axis shows little bending, with the plane of the pyrene ring system perpendicular to the helical axis. The hydrocarbon is stacked under the dG_{15}−dC_4 base pair and over dA_5, to which it is covalently bonded (Figure 6). The base of dG_{14} at the GA mismatch is turned out into the major groove (Figure 6). The hydrocarbon opens the minor groove and reduces the average helical twist with

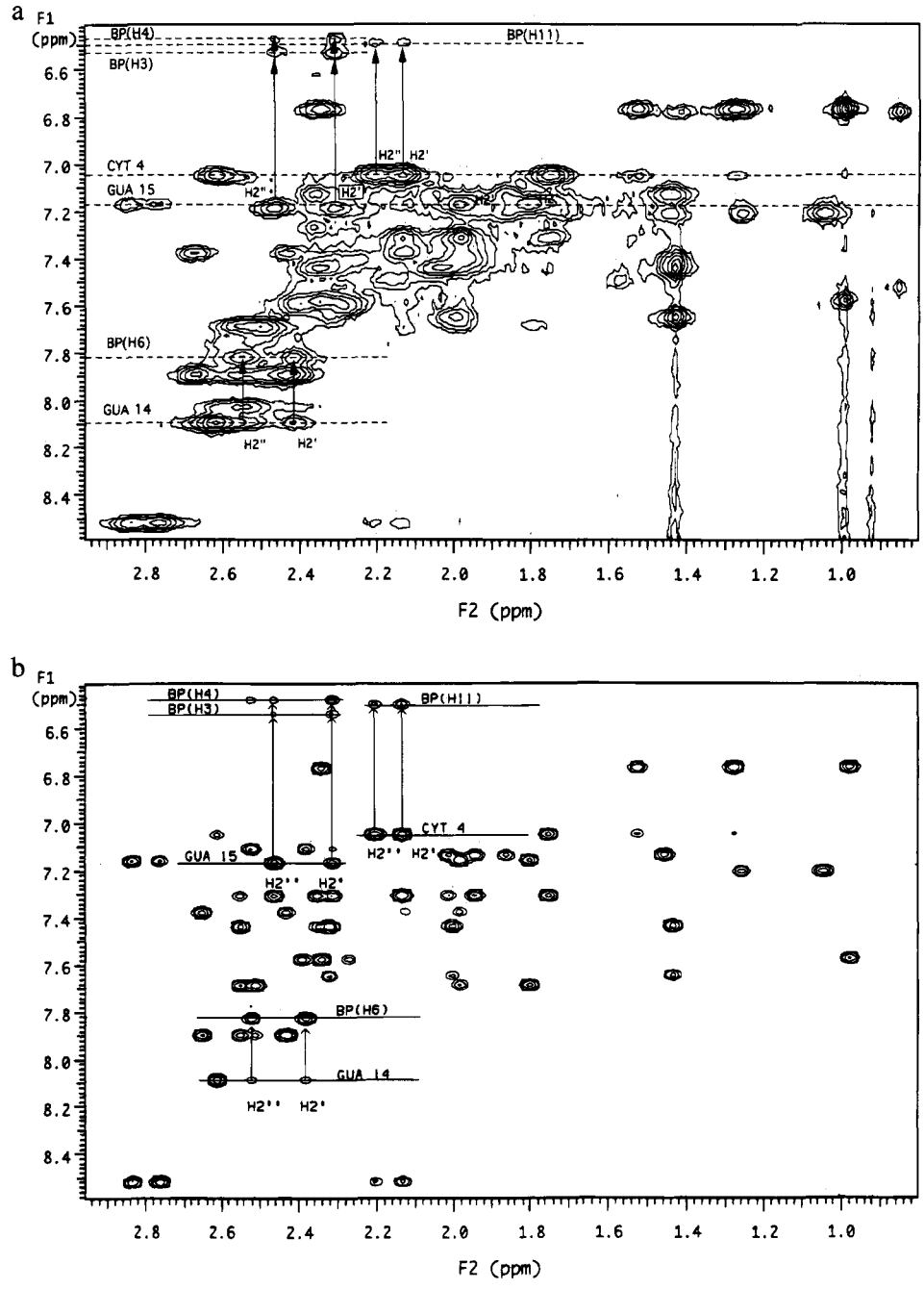

FIGURE 9: (a) Expanded NOESY spectrum (150 ms mixing time) showing the cross peaks for base protons (6.5 to 8.6 ppm) and sugar H2′ and H2″ protons (1.0 to 2.9 ppm). The base protons for nucleotides that have NOEs to hydrocarbon protons are indicated with horizontal dashed lines. Sugar H2′,H2″ to hydrocarbon proton NOEs are indicated with arrows. (b) Expanded simulated NOESY spectrum (150 ms mixing time) for the same base to H2′,H2″ region as part a. Simulation shows the reproduction of long distance NOEs between the hydrocarbon protons and the DNA sugar protons.

an overall 10.7 base pairs per turn from 10.0 base pairs per turn of the model-built unmodified B-DNA duplex.

Comparison of Simulated NOESY and Experimental Spectra. The refined structure was used with MORASS to simulate the NOESY spectra at the 150 ms mixing time. The simulation duplicated the weak NOEs between the tetrahydro-BaP moiety and the DNA backbone sugars (dC_4, dG_{14}, and dG_{15}), which established the intercalated orientation of the hydrocarbon (Figure 9a,b). The simulation also shows the same break between dG_{14} and dG_{15} as in the experimental NOESY spectra. Other parts of the experimental and simulated spectra show a high degree of homology.

DISCUSSION

Melting temperatures of duplexes of the two isomeric oligonucleotides containing adducts (Figure 1) derived from trans addition of the exocyclic amino group of dA to (−)-(7*S*,8*R*,9*R*,10*S*)-7,8-dihydroxy-9,10-epoxy-7,8,9,10-tetrahydrobenzo[*a*]pyrene and (+)-(7*R*,8*S*,9*S*,10*R*)-7,8-dihydroxy-9,10-epoxy-7,8,9,10-tetrahydrobenzo[*a*]pyrene [(−)- and (+)-BaP-DE2)] with both normal (T) and mispaired purine bases opposite the modified dA residue are shown in Table 1. For NMR studies, we selected a duplex in which a dG residue is opposite the modified dA, since the T_m for the *trans*-(+)-DE2 (10*S*)-dA adduct with dG opposite the adduct is more

than 10 deg higher than that for the corresponding duplex with T opposite the adduct. This suggested that some specific structural features associated with the enhanced stability of this base mismatch might lead to insights into mechanisms of diol epoxide-induced mutagenesis. To investigate the effect of the stereochemistry of the bound diol epoxide on the solution conformations of these structures, we have undertaken to examine the same mispaired duplexes derived from both enantiomers of BaP-DE2. Unlike the (10*S*)-dA adduct from the (+)-(7*R*,8*S*,9*S*,10*R*)-DE2 adduct, the (10*R*)-dA adduct from the (−)-(7*S*,8*R*,9*R*,10*S*)-DE2 adduct with dG opposite the modified dA, which is the subject of the present study, does not exhibit enhanced thermal stability relative to the duplex with T opposite the adduct, presumably because the duplex containing T is markedly more stable when the dA adduct is derived from the (−)-DE2 as opposed to the (+)-DE2 enantiomer.

The NOE refined structure of the nonamer duplex d(GGTCA*CGAG)·d(CTCGGGACC) with A*, corresponding to the *trans*-(−)-DE2 (10*R*)-dA adduct, was determined to have the hydrocarbon intercalated between the fourth and sixth base pairs. The hydrocarbon was stacked in from the major groove, with the base of dG_{14} (dG of the GA mismatch) turned out into the major groove. NOE cross peaks between protons on the hydrocarbon and those on the DNA duplex established this orientation, which was further supported by chemical shift patterns near the hydrocarbon. The minor conformer was in slow exchange, and only the most intense minor conformer peaks were observable. Slow exchange was not unexpected because repositioning of the hydrocarbon, modified dA*, or other bases would require partial melting of the duplex with an associated high activation barrier.

Structural NMR studies of oligonucleotides containing the trans opened (10*S*)-dG and (10*R*)-dG adducts and a cis opened (10*R*)-dG adduct from BaP-DE2 (Cosman et al., 1992, 1993a; de los Santos et al., 1992) provide structural support for earlier optical spectroscopic studies that suggested a two-site classification scheme (Geacintov et al., 1982; Zinger et al., 1987; Harvey & Greacintov, 1988; Graslund & Jernstrom, 1989; Jankowiak et al., 1990). Site I adducts are intercalated, whereas site II adducts are solvent-exposed. The site II adducts have the hydrocarbon in the minor groove directed toward the 3′- or 5′-end of the modified strand and the covalently modified dG is stacked in. Optical studies of oligonucleotides containing cis and trans opened dG adducts from BaP-DE2 show that the cis opened isoemrs of the dG adducts favor the site I position (Geacintov et al., 1990, 1991).

Currently, NMR structures of oligonucleotides containing three out of the eight possible dG adducts from BaP-diol epoxides have been solved (Figure 10a,b), and the structure of a fourth BaP dG adduct has also been suggested (Figure 10a,b). Further, two NMR structures out of the eight possible dA adducts from BaP-diol epoxides have been investigated by our laboratories (Figure 10a,b). As more structural information for BaP dG and dA adducts is obtained, hopefully it will be possible to explain rationally why the hydrocarbon intercalates in some of these structures but not in others. Predictions for the structures of dG and dA adducts from BaP-diol epoxides should be possible.

The van der Waals radius of the aromatic part of the hydrocarbon is approximately the same as a base pair, and the local interaction with nearest-neighbor base pairs is limited. For effective intercalation, the plane of the pyrene moiety must be perpendicular to the helical axis (observed in all intercalated structures). Further, slight crowding of the hydrocarbon to the top or bottom (top is defined as the 5′-direction of the modified strand) of the site of intercalation will result in steric interactions between its hydroxyl groups and the nucleotides above or below. When the hydroxyls on the tetrahydro-BaP are in the major groove (such as in our intercalated dA adduct), then these hydroxyls can avoid steric crowding by being toward the top of the site. When the tetrahydro-BaP hydroxyls are in the minor groove (intercalated BaP dG adduct), then these hydroxyls can avoid steric crowding by orienting toward the bottom of the site. These steric interactions would be expected to be most acute for intercalated BaP dG (tetrahydro-BaP hydroxyls in the minor groove), as opposed to intercalated BaP dA adducts (tetrahydro-BaP hydroxyls in the major groove).

The effect of these steric interactions is illustrated in the solved structures of two oligonucleotides containing dA adducts of BaP-diol epoxides (Figure 10a,b). Intercalation of the hydrocarbon from the major groove with the dA stacked in puts the three hydroxyl groups of the tetrahydro-BaP in the relatively wide major groove and the aromatic end partially stacked over the covalently linked dA. The *R* chirality at C10 in the present structure places the hydroxyls on the hydrocarbon moiety toward the top of the site of intercalation, with dA in the anti conformation. This minimizes steric interactions between the tetrahydro-BaP hydroxyls and the nucleotides at the site of intercalation. For the adduct derived from the enantiomeric (+)-BaP-DE2 by trans ring opening, the resultant *S* chirality at C10 would place the tetrahydro-BaP hydroxyls toward the bottom of the intercalation site (resulting in steric crowding) when dA is anti. This conformation is not observed. Instead, the dA flips to the syn conformation (Yeh et al., manuscript in preparation), which moves the hydroxyls on the hydrocarbon farther out into the major groove (removing some of the steric crowding) but still allows the aromatic end to intercalate. This anti to syn dA ring flip for the (10*S*)-DE2 adduct could explain the 12 °C lower melting temperature of the adduct with a complementary T opposite relative to the (10*S*)-DE2 adduct with a dG mismatch (Table 1, 28 °C for x = dG vs 16 °C for x = T).

This suggests that chirality at C10 can be used to predict whether the dA will be syn (C10 is *S*) or anti (C10 is *R*) for dA adducts in which the tetrahydro-BaP moiety is intercalated. Further, the ability of dA to change conformation to relieve unfavorable steric interactions associated with the tetrahydro hydroxyls, coupled with the space in the major groove, suggests that the chiral centers at C9, C8, and C7 are unimportant for determining intercalation. Application of the working hypothesis developed earlier predicts that the remaining dA adducts derived from BaP-diol epoxides will also be intercalated. An oligonucleotide containing a (10*R*)-dA adduct derived from the enantiomer of BcPh-DE2 with the same absolute configuration as the BaP-DE2 in this study also follows these predictions (Cosman et al., 1993). Thus, the modified dA is in the anti configuration with the tetrahydro-BcPh intercalated above the dA.

A brief look at the solved structures for the BaP dG adducts makes it apparent that the chirality of C10 alone cannot be used to predict the geometry of the hydrocarbon

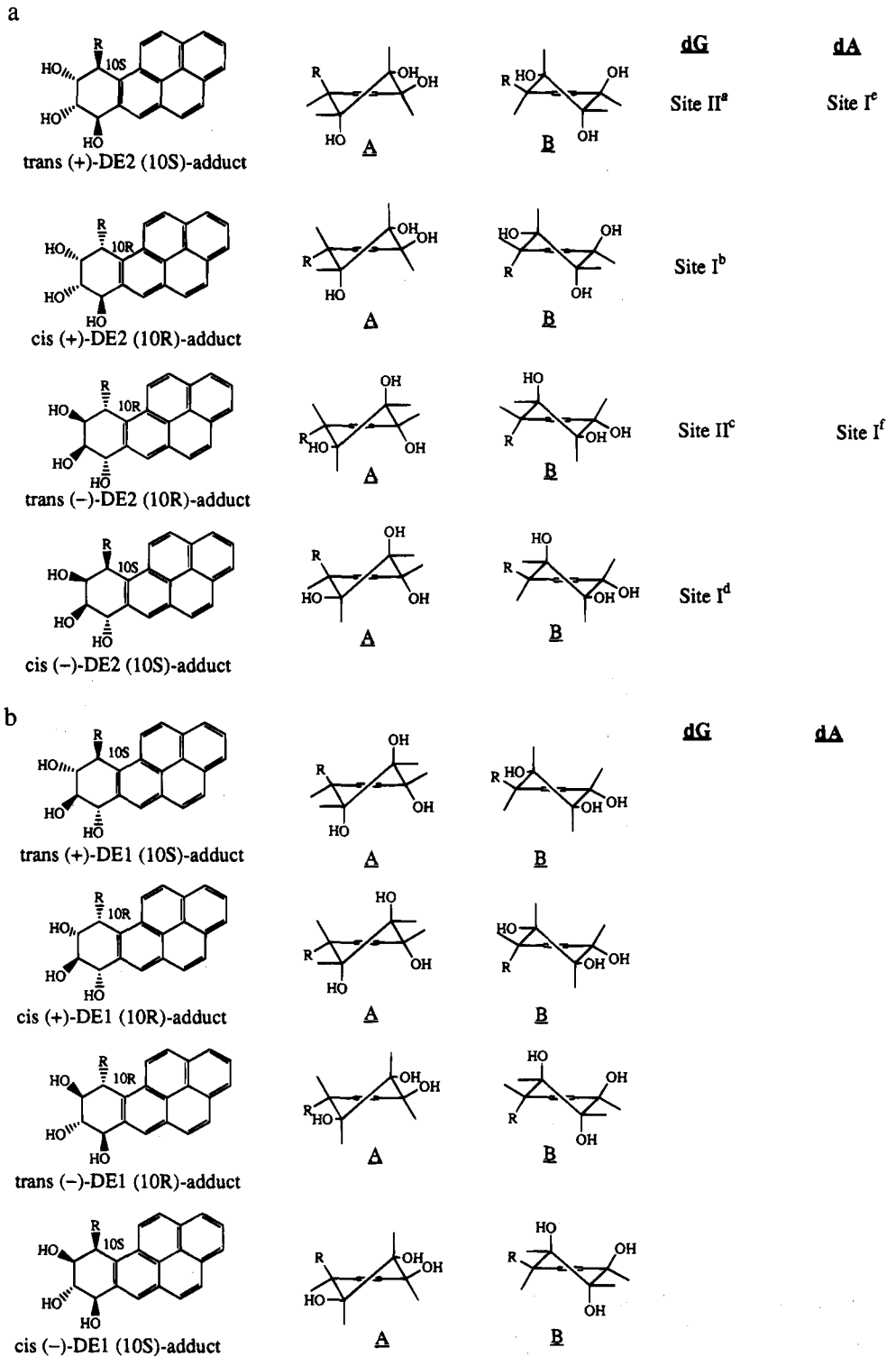

FIGURE 10: Absolute configurations of the eight possible dG and dA adducts from BaP-DE1 and -DE2. The aliphatic ring of the hydrocarbon in each adduct can assume two conformational isomers, as shown. [a]Cosman et al., 1992. [b]Cosman et al., 1993a. [c]De los Santos et al., 1992. [d]Geacintov et al., 1990, 1991. [e]Unpublished work (Yeh et al., manuscript in preparation). [f]Subject of current work.

in dG adducts. The adduct derived from cis ring opening of (7*R*,8*S*,9*S*,10*R*)-DE2 and that derived from trans ring opening of (7*S*,8*R*,9*R*,10*S*)-DE2 both have the same absolute configuration at C10 (*R*), but only the first is intercalated. Similarly, the adducts derived from trans ring opening of (7*R*,8*S*,9*S*,10*R*)-DE2 and cis ring opening of (7*S*,8*R*,9*R*,10*S*)-DE2 have the same chirality at C10 (*S*), but the second adduct is believed to be intercalated whereas in the first adduct the hydrocarbon is located in the minor groove. Since the hydroxyls of the hydrocarbon are now in the restricted space of the minor groove, it is not unexpected that the chiral centers at C9, C8, and C7 and possibly the conformation of the aliphatic ring itself can affect the orientation of the intercalated hydrocarbon.

The role of the chiral centers other than C10 in affecting intercalation geometry can be seen with the (10*R*)-dG adducts resulting from the cis ring opening of (7*R*,8*S*,9*S*,10*R*)-DE2 and trans ring opening of (7*S*,8*R*,9*R*,10*S*)-DE2. The 10*R* absolute configuration for the intercalated *cis*-DE2 adduct places the tetrahydro-BaP hydroxyls toward the bottom of

the site, near the modified strand and in the minor groove (Cosman et al., 1993a). The plane of the modified dG is turned parallel to the helical axis. The aliphatic ring is in conformation B (Figure 10a,b), and the chirality at C9 and C8 points the hydroxyls away from the nucleotide below it. The same (*R*) chirality at C10 for the trans adduct from the enantiomeric DE2 would allow it to enter the same intercalation position, but it does not intercalate (Cosman et al., 1993a). This can be rationalized because if the *trans*-DE2−(10*R*)-dG adduct assumes the same B conformation, the C9 hydroxyl becomes axial and sticks into the nucleotide below. Conformation A for this adduct places the C8 hydroxyl axial, again sticking into the nucleotide below. This inability to assume a conformation that alleviates these unfavorable steric interactions would disfavor intercalation.

Evidence suggests that the (10*S*)-dG adduct resulting from the cis opening of (7*S*,8*R*,9*R*,10*S*)-DE2 is intercalated (Geacintov et al., 1990, 1991). Intercalation is possible with the dG in the anti configuration, placing the hydrocarbon hydroxyls at the bottom of the site in the minor groove. These hydroxyl groups would also be displaced toward the unmodified strand. The same dG orientation that is in the intercalated *cis*-DE2−(10*R*)-dG adduct derived from the enantiomeric diol epoxide is not possible because it would put the hydrocarbon into direct contact with the base pair at the top of the site of intercalation. In both the A and B conformations of the *cis*-DE2−(10*S*)-dG adduct, HO9 and HO8 are pointed away from the nucleotide above on the unmodified strand. The chirality at C10 (*S*) of the *trans*-DE2−(10*S*)-dG adduct would allow it to enter the same intercalation position as the *cis*-DE2−(10*S*)-dG adduct, but it does not intercalate (Cosman et al., 1992). This is because both the A and B conformations of the *trans*-DE2−(10*S*)-dG adduct place the hydroxyl at either C9 or C8 axial, sticking into the nucleotide above.

Although no NMR studies of oligonucleotides containing dG adducts derived from BaP-DE1 are presently available, some speculative predictions are possible concerning the likelihood of intercalation of the four possible DE1 dG adducts. Following the preceding considerations, we suggest that, for dG adducts with *R* absolute configuration at C10, intercalation will be disfavored by axial C8 or C9 hydroxyl groups above the plane of the ring system when it is oriented as shown in Figure 10; similarly, for dG adducts with *S* absolute configuration at C10, intercalation will be disfavored by axial hydroxyl groups below the plane. (Note that the orientation of the ring system shown in Figure 10 is opposite that used in describing its position relative to its DNA intercalation sites.) Both the (10*S*)- and (10*R*)-dG adducts derived from cis opening of the two enantiomers of DE1 can assume conformations [A for the cis (10*R*) adduct and B for the cis (10*S*) adduct] in which all hydroxyl groups are equatorial and steric interactions unfavorable to intercalation are avoided. Thus, we predict that the hydrocarbon will intercalate in oligonucleotides containing either of the *cis*-DE1 adducts. For each of the two adducts derived from trans opening of the DE1 enantiomers, the preferred conformation is likely to have the purine substituent in a pseudoaxial orientation to avoid unfavorable steric interactions in the bay region of the hydrocarbon (Cheh et al., 1993; Sayer et al., 1991; Cheng et al., 1989). This would place the C8 hydroxyl in an unfavorable orientation for intercalation [conformation A of the *trans*-DE1−(10*S*)-dG adduct or conformation B of the *trans*-DE1−(10*R*)-dG adduct]. Thus, we predict that the hydrocarbon in these adducts will not intercalate. Other factors, such as the possible effects of neighboring bases and base mispairs, such as that described in the present study, on the relative stability of intercalated vs groove-bound structures, may also influence the geometry of the isomeric dA and dG adducts from the four optically active BaP-diol epoxides and remain to be investigated.

SUPPLEMENTARY MATERIAL AVAILABLE

The supplementary material contains a 100 ms TOCSY spectrum of the dC H5 to H6 region (Figure 1S), which shows evidence for the presence of the minor conformer. Also included are 150 ms NOESY spectra of the base (H6, H8) to H2′,H2″ region for the modified and unmodified oligonucleotide strands (Figures 2S and 3S). These spectra show additional cross peaks to the hydrocarbon ring (7 pages). Ordering information is given on any current masthead page.

REFERENCES

Bax, A., & Davis, D. G. (1985) *J. Magn. Reson. 65*, 355−360.

Boelens, R., Koning, T., & Kaptein, R. (1988) *J. Mol. Struct. 173*, 299−311.

Boelens, R., Koning, T., van der Marel, G., van Boom, J., & Kaptein, R. (1989) *J. Magn. Reson. 82*, 290−308.

Braunschweiler, L., & Ernst, R. R. (1983) *J. Magn. Reson. 71*, 521.

Cheh, A. M., Chadha, A., Sayer, J. M., Yeh, H. J. C., Yagi, H., Pannell, L. K., & Jerina, D. M. (1993) *J. Org. Chem. 58*, 4013−4022.

Cheng, S. C., Hilton, B. D., Roman, J. M., & Dipple, A. (1989) *Chem. Res. Taxicol. 2*, 334−340.

Cosman, M., Ibanez, V., Geacintov, N. E., & Harvey, R. G. (1990) *Carcinogenesis 11*, 1667−1672.

Cosman, M., de los Santos, C., Fiala, R., Hingerty, B. E., Sigh, S. B., Ibanez, V., Margulis, L., Live, D., Geacintov, N. E., Broyde, S., & Patel, D. J. (1992) *Proc. Natl. Acad. Sci. U.S.A. 89*, 1914−1918.

Cosman, M., de los Santos, C., Fiala, R., Hingertz, B. E., Ibanez, V., Luna, E., Harvey, R., Geacintov, N. E., Broyde, S., & Patel, D. J. (1993a) *Biochemistry 32*, 4145−4155.

Cosman, M., Fiala, R., Hingerty, B. E., Laryea, A., Lee, H., Harvey, R. G., Amin, S., Geacintov, N. E., Broyde, S., & Patel, D. J. (1993b) *Biochemistry 32*, 12488−12497.

De los Santos, C., Cosman, M., Hingerty, B. E., Ibanez, V., Margulis, L. A., Geacintov, N. E., Broyde, S., & Patel, D. J. (1992) *Biochemistry 31*, 5245−5252.

Geacintov, N. E., Giagliano, A. G., Ibanez, V., & Harvey, R. G. (1982) *Carcinogenesis 3*, 247−253.

Geacintov, N. E., Cosman, M., Ibanez, V., Birke, S. S., & Swenberg, C. E. (1990) in *Molecular Basis of Specificity in Nucleic Acid Drug Interactions* (Pullman, B., & Jortner, J., Eds.) pp 443−450, Kluwer Academic Publishers, Dordrecht, The Netherlands.

Geacintov, N. E., Cosman, M., Mao, B., Alfano, A. A., Ibanez, V., & Harvey, R. G. (1991) *Carcinogenesis 12*, 2099−2108.

Gorenstein, D. G., Meadows, R., Metz, J. T., Nickonowicz, E., & Post, C. B. (1990) *in Advances in Biophysical Chemistry* (Bush, C. A., Ed.) JAI Press, Greenwich, CT.

Gorenstein, D. G., Luxon, B. A., Post, C. B., & Meadows, R. (1993) *MORASS2.0* Program.

Graslund, A., & Jernstrum, B. (1989) *Q. Rev. Biophys. 22*, 1−37.

Harvey, R. G., & Geacintov, N. E. (1988) *Acc. Chem. Res. 21*, 2279−2299.

Hingerty, B. E., & Broyde, S. (1985) *Biopolymers 24*, 2279−2299.

James, T. L., Thomas, P. D., & Basos, V. J. (1991) *Proc. Natl. Acad. Sci. U.S.A. 88* (4), 1237−41.

Jankowiak, R., Lu, P. Q., Small, G., & Geacintov, N. E. (1990) *Chem. Res. Toxicol. 3*, 39−46.

Jerina D. M., Cheh, A. M., Chadha, A., Yagi, H., & Sayer, J. M. (1988) in *Macrosomes and Drug Oxidations*: Proceedings *of the 7th International Symposium* (Miners, J. O., Brikett, D. J., Drew, R., May, B. K., & McManus, M. E., Eds.) pp 354−362, Taylor and Francis, London.

Jerina, D. M., Chadha, A., Cheh, A. M., Schurdak, M. E., Wood, A. W., & Sayer, J. M. (1991) in *Biological Reactive Intermediates IV. Molecular and Cellular Effects and their Impact on Human Health* (Wittmer, C. M., Snyder, R., Jollow, D. J., Kalf, G. F., Kocsis, J. J., & Sipes, I. G., Eds.) pp 533−553 and references therein, Plenum Press, New York.

Kaluarachchi, K., Meadows, R. P., & Gorenstein, D. G. (1991) *Biochemistry 30*, 8785−8797.

Lakshman, M. K., Sayer, J. M., Yagi, H., & Jerina, D. M. (1992) *J. Org. Chem. 57*, 4585−4590.

Langridge, R., & Ferrin, T. E. (1984) *J. Mol. Graphics 2*, 56.

Nickonowicz, E., Meadows, R., Post, C., Jones, C., & Gorenstein, D. G. (1989) *Bull. Magn. Reson. 11*, 226−229.

Nickonowicz, E., Meadows, R., & Gorenstein, D. G. (1990) *Biochemistry 29*, 4193−4204.

Sayer, J. M., Chadha, A., Agarwal, S. K., Yeh, H. J. C., Yagi, H., & Jerina, D. M. (1991) *J. Org. Chem. 56*, 20−29.

Wei, S.-J. C., Chang, R. L., Wong, C.-Q., Bhachech, N., Cui, X. X., Hennig, E., Yagi, H., Sayer, J. M., Jerina, D. M., Preston, B. D., & Conney, A. H. (1991) *Proc. Natl. Acad. Sci. U.S.A. 88*, 11227−11230.

Wei, S.-J. C., Chang, R. L., Bhachech, N., Cui, X. X., Merkler, K. A., Wong, C.-Q., Hennig, E., Yagi, H., Jerina, D. M., & Conney, A. H. (1993) *Cancer Res. 53*, 3294−3301.

Wei, S.-J. C., Chang, R. L., Hennig, E., Cui, X. X., Merkler, K. A., Wong, C.-Q., Yagi, H., Jerina, D. M., & Conney, A. H. (1994) *Carcinogenesis* (in press).

Weiner, P. K., & Kollman, P. A. (1981) *J. Comput. Chem. 2*, 287−303.

Wüthrich, K. (1986) *NMR of Proteins and Nucleic Acids*, Wiley, New York.

Zinger, D., Geacintov, N. E., & Harvey, R. G. (1987) *Biophys. Chem. 27*, 131−138.

BI940289V